communications earth & environment

Article

A Nature Portfolio journal

https://doi.org/10.1038/s43247-025-02123-5

Evidence for Atlantic Ocean forcing the atmosphere and the negative role of model bias

Rein Haarsma [1,2] & Sybren Drijfhout[2,3]

There is agreement on how the North Atlantic Oscillation forces the Atlantic Meridional Overturning Circulation, but the existence of a reversed interaction is widely disputed. Here, we investigate this type of ocean forcing the atmosphere by analysing several high- and low-resolution coupled climate models, ocean observations and reanalyses products of ocean and atmosphere. We find that in observations and about 50% of the coupled climate models, an ocean-forced negative North Atlantic Oscillation occurs at a lag of 5 years after the Atlantic Meridional Overturning Circulation peaks. Climate models with a strong cold temperature bias in the subpolar gyre and a positive sea-ice cover bias in the Atlantic and Arctic Ocean are unable to correctly simulate the heat flux pattern, resulting from the northward propagation of warm ocean temperatures, that forces the atmosphere. Efforts to remove this bias could therefore lead to substantial improvement in current decadal prediction systems.

The North Atlantic Oscillation (NAO) forces Atlantic Meridional Overturning Circulation (AMOC) variations on different timescales, depending on whether wind or buoyancy forcing is addressed. The relevant mechanisms through which the NAO impacts the AMOC can be disentangled by discriminating between intraseasonal, interannual and decadal fluctuations. On shorter timescales wind forcing dominates through eastern boundary upwelling by Ekman pumping, creating density anomalies that drive changes in the AMOC. A delayed response is also seen where Rossby waves, excited at the eastern boundary, travel westward and impact the western boundary density. At decadal timescales buoyancy forcing dominates, affecting the stratification in the subpolar gyre (SPG) and deep-water formation (DWF). On interannual timescales both wind and buoyancy forcing are important[1].

Earlier studies, focusing on longer timescales used NAO-derived buoyancy fluxes to demonstrate that variability in a coupled model can be largely recovered by an ocean only model using low-passed buoyancy fluxes, mainly heat fluxes[2]. When projecting such fluxes on the NAO index it was shown that it was mainly the NAO that forced the AMOC[3,4]. On shorter timescales wind variations related to the NAO were also found to be dominant in explaining short-term variations in the RAPID-data[5,6].

A reversed interaction, namely AMOC impacting the NAO, is less clear and more controversial. In the CCSM3 model, it was shown that after AMOC intensification a horseshoe pattern in SST develops that on long timescales is correlated with the Atlantic multidecadal variability (AMV)[7], invoking a negative NAO response. A weak negative NAO response on multidecadal timescales was also detected in a multi-model analysis[8]. This interaction was further corroborated by using AMOC-related SST (AMV) patterns to force the NAO[9,10] and supported by data analysis[11].

The AMOC–AMV link, however, was in the last decade challenged[12–16], although a recent comprehensive review concluded that the AMOC–AMV link does exist[17] and that observed and modelled subsurface fingerprints of AMV-variability are inconsistent with the hypothesis that the AMV is solely forced by radiative processes or stochastic noise. It was noted, however, that model bias severely hinders a thorough understanding of this link and that many climate models have difficulty in correctly simulating the observed AMV[17]. The link between AMV and (wintertime) NAO is severely underestimated in most models[18,19], and as a result, the multidecadal variability in NAO is underestimated as well[20,21]. For this reason, it was hypothesised that model bias may be a reason for the inconsistent NAO response to AMOC/AMV fluctuations in climate models[17]. Recent studies confirmed this to be the case for the AMOC response to NAO forcing[22,23]. The enhanced SIC and stratification induced by a cold bias in the northern North Atlantic results in reduced DWF in the Nordic Seas and thereby reduced forcing of the AMOC.

Here, we address using an ensemble of the most recent models with the highest resolution (High Resolution Model Intercomparison Project (HighResMIP)) ("Data and methods" section), the relation between model

[1]Barcelona Supercomputing Center (BSC), Barcelona, Spain. [2]Royal Netherlands Meteorological Institute (KNMI), De Bilt, The Netherlands. [3]University of Southampton, Southampton, UK. e-mail: reindert.haarsma@bsc.es

bias and NAO–AMOC interaction, focusing on the still controversial NAO response to AMOC variations. Until now most analyses of the full NAO–AMOC coupling, especially including NAO forcing by the ocean have been limited to single model studies[24], and with models hampered by large biases[8,25] leading to variable and inconclusive results. In addition, we compare this interaction with observations and reanalyses (RAPID, ERA5 and ORAS5) ("Data and methods" section). We argue that model bias may affect the strength of the AMOC response to NAO forcing, but that this type of forcing and response is qualitatively well simulated in most climate models. How model bias affects the lagged NAO response to the AMOC is more controversial, with some studies pointing towards a lagged negative NAO response and a warming of the SPG, while others do not confirm this relation[11,26,27]. Our results explain this disagreement, which appears associated with model bias and its impact on convective mixing and DWF.

Results

Relationship between AMOC strength and NAO

The cross-correlation analyses of the AMOC strength at 26.5° N with the normalised winter NAO index, the SST in the SPG and the mixed-layer depth (MLD) in the Labrador Sea, which is used here as a proxy for DWF ("Data and methods" section), reveal a large spread among the models (Fig. 1). Based on their NAO behaviour and their similarity with RAPID-ERA5, we have divided the models in two groups NAO− (7 models) and NAO+ (8 models). The NAO− models have a negative NAO around lag +5 (positive lag is when the variable lags the AMOC, negative when it leads the AMOC), as is the case in the RAPID-ERA5 data, with a positive SST anomaly in the SPG, and enhanced MLD in the Labrador Sea around lag −3. The NAO+ group does not reveal this behaviour. The main difference between NAO− and RAPID-ERA5 is, apart from the higher correlations of

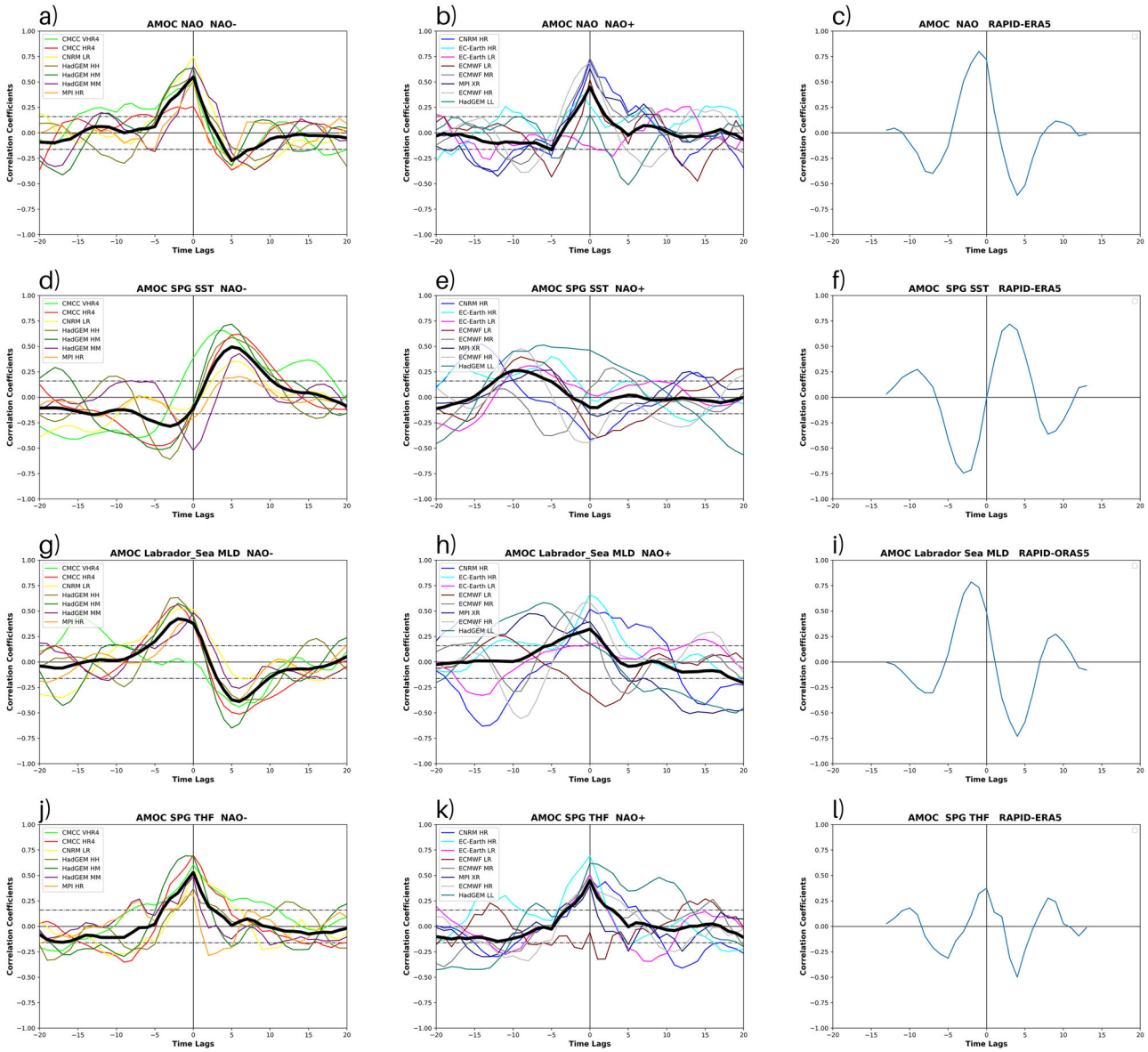

Fig. 1 | Cross-correlations between AMOC strength and state indices. Cross-correlation between the AMOC strength at 26.5° N for different lags with **a**–**c** the normalised NAO index ("Data and methods" section), **d**–**f** SST averaged over the SPG (45 W–20 W, 45 N–65 N), **g**–**i** MLD averaged over the Labrador Sea (80 W–40 W, 50 N–80 N) and **j**–**l** THF averaged over the SPG (positive lag when the variable lags AMOC, negative when it leads the AMOC, THF is defined as positive when upward). NAO− models (**a**, **d**, **g**, **j**), NAO+ models (**b**, **e**, **h**, **k**), RAPID-ERA5/ORAS5 (**c**, **f**, **i**, **l**). The thick black lines denote the model mean of the NAO− and NAO+ groups. The correlations are computed for the winter season (DJF) with a running mean of 5 years. The dashed horizontal lines denote the 95% significance values of the multi-model mean ("Data and methods" section). Due to the short RAPID-ERA5/ORAS5 time series no significance level could be assigned there.

the latter, that the cross-correlation with the NAO index for the NAO− group peaks at lag 0, whereas for RAPID-ERA5 around lag −3. The buoyancy forcing (latent + sensible heat flux), which drives the changes in MLD associated with DWF, peaks around lag −3 for both NAO− and RAPID-ERA5 (Fig.1g, i). The regression at lag −3 of the buoyancy forcing on the AMOC is, however, weaker in the NAO− models than in RAPID-ERA5 (Fig. S1a, c). The wind-driven forcing (taux), which is maximum at lag 0, is on the other hand of the same value for the NAO− models and RAPID-ERA5 (Fig. S1d, f). This explains why the positive correlation between AMOC and NAO is in phase for the NAO− group and around lag −3 in RAPID-ERA5 (Fig. 1a, c). Repeating the analyses using OAFlux[28] instead of ERA5 fluxes confirmed this (Fig. S1g, h). However, for the AMOC strength between 30 and 50 N, the NAO− models also peak at lag −3 (Fig. S2). To be able to compare model results with RAPID-ERA5, we will show only results for AMOC at 26.5° N. A notable outlier in the NAO− group is CMCC-VHR4, which does not show enhanced MLD in the SPG at lag −3 (Fig. 1g). This model, however, features enhanced MLD in the Nordic Seas at lag −3 (not shown). Together with its negative NAO peak at lag +5, this motivated us to include it in the NAO− group.

Based on the above cross-correlation analyses, where NAO− and RAPID-ERA5/ORAS5 reveal coherent and notable peaks at lags −3 (AMOC–SST and AMOC–MLD), 0 (AMOC–NAO and AMOC–THF) and +5 (all cross-correlations) we will focus in the rest of the paper on these lags. We plotted the model mean of the regression of the mean sea-level pressure (MSLP) on the AMOC for these lags for the NAO− and NAO+ groups and RAPID-ERA5 (Fig. 2). NAO− and RAPID-ERA5 reveal a strong resemblance although regressions for RAPID-ERA5 are substantially higher. For NAO+ the response is positive at both positive and negative lags, but weaker at negative lags compared with NAO− and RAPID-ERA5. Both model groups and RAPID-ERA5 show a strong and similar response at lag 0. Further analyses (not shown) revealed that this is largely due to the Ekman response, in agreement with earlier studies[1].

Mechanism of NAO forced by the AMOC at positive lag

NAO− reveals a strong SST warm signal at positive lag in the SPG that is absent in NAO+ but also observed in RAPID-ERA5. In the latter, the warm SSTs extend into the Labrador Sea, an extension of the warm anomaly pattern that is absent in the models (Fig. 3a, g). In contrast, NAO+ reveals prominent warm SSTs in the Gulf Stream in the neighbourhood of Cape Hatteras, which is absent in NAO− and RAPID-ERA5.

Comparing regression plots between AMOC and THF (Fig. 3b), which is here defined as positive if it is upward, with those between AMOC and SST (Fig. 3a) reveal that the warm SPG-SSTs in NAO− are forced by the ocean, because the atmosphere is cooling the ocean in this region. The oceanic heat convergence in the SPG at positive lags has also been noted in other studies[24,29]. The SPG in RAPID-ERA5 is warmed by the atmosphere, but substantially less than the Labrador Sea that has similar warm SSTs as in the SPG (Fig. 3g, h) indicating that in the SPG part of the warm SSTs is due to the warming by ocean advection. The SST/THF regression for the longer ERA5 periods (1981–2023), being the satellite era, and even the whole ERA5

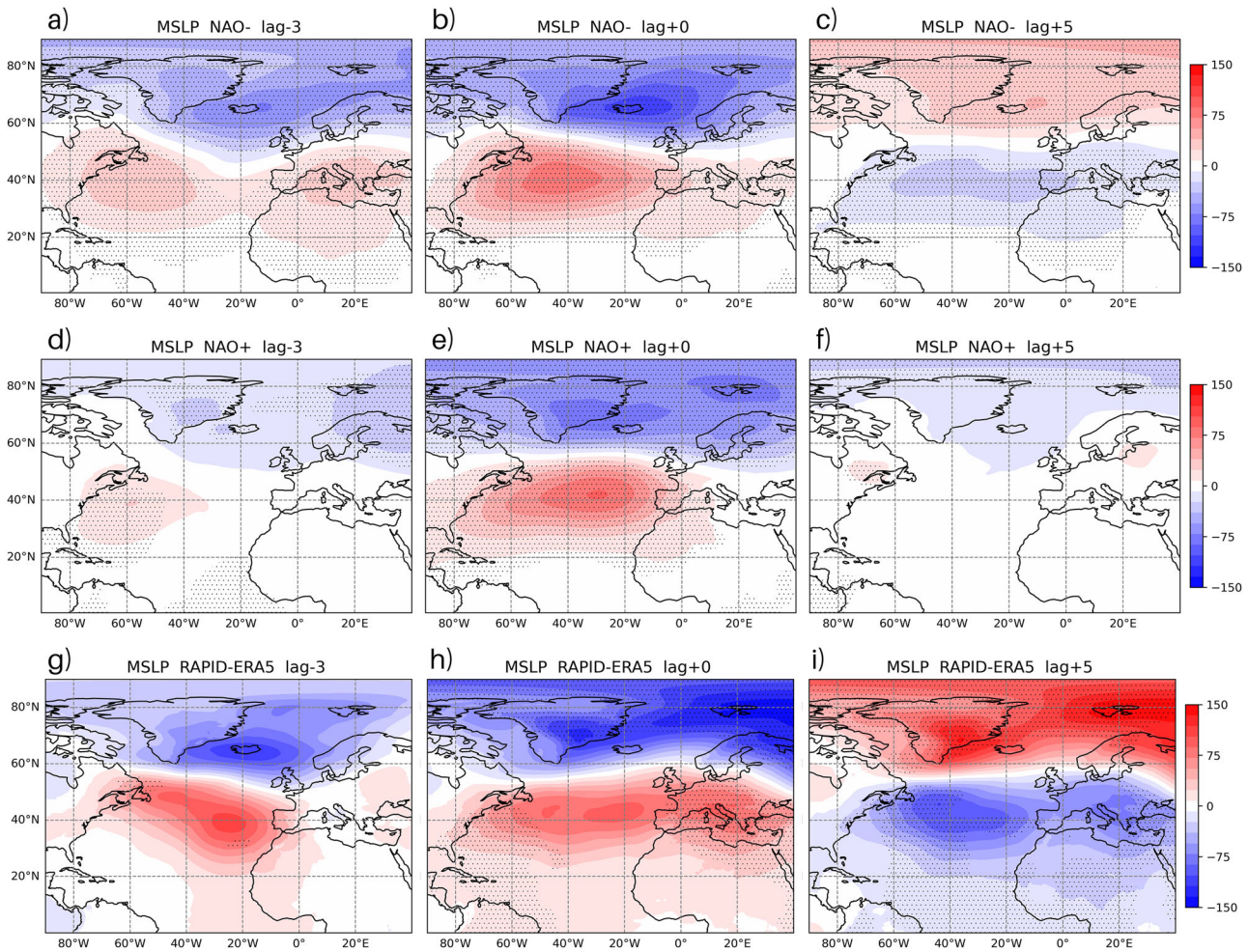

Fig. 2 | Regression AMOC strength on MSLP. Regression of AMOC strength at 26.5° N on MSLP (Pa Sv^{-1}). **a**–**c** Model mean of NAO− models; **d**–**f** model mean of NAO+ models; **g**–**i** RAPID-ERA5. **a**, **d**, **g**, lag −3. **b**, **e**, **h** lag 0. **c**, **f**, **i** lag +5. The regressions are computed for the winter season (DJF) with a running mean of 5 years. Areas of statistical significance with a p value < 0.05 are indicated by stippling ("Data and methods" section).

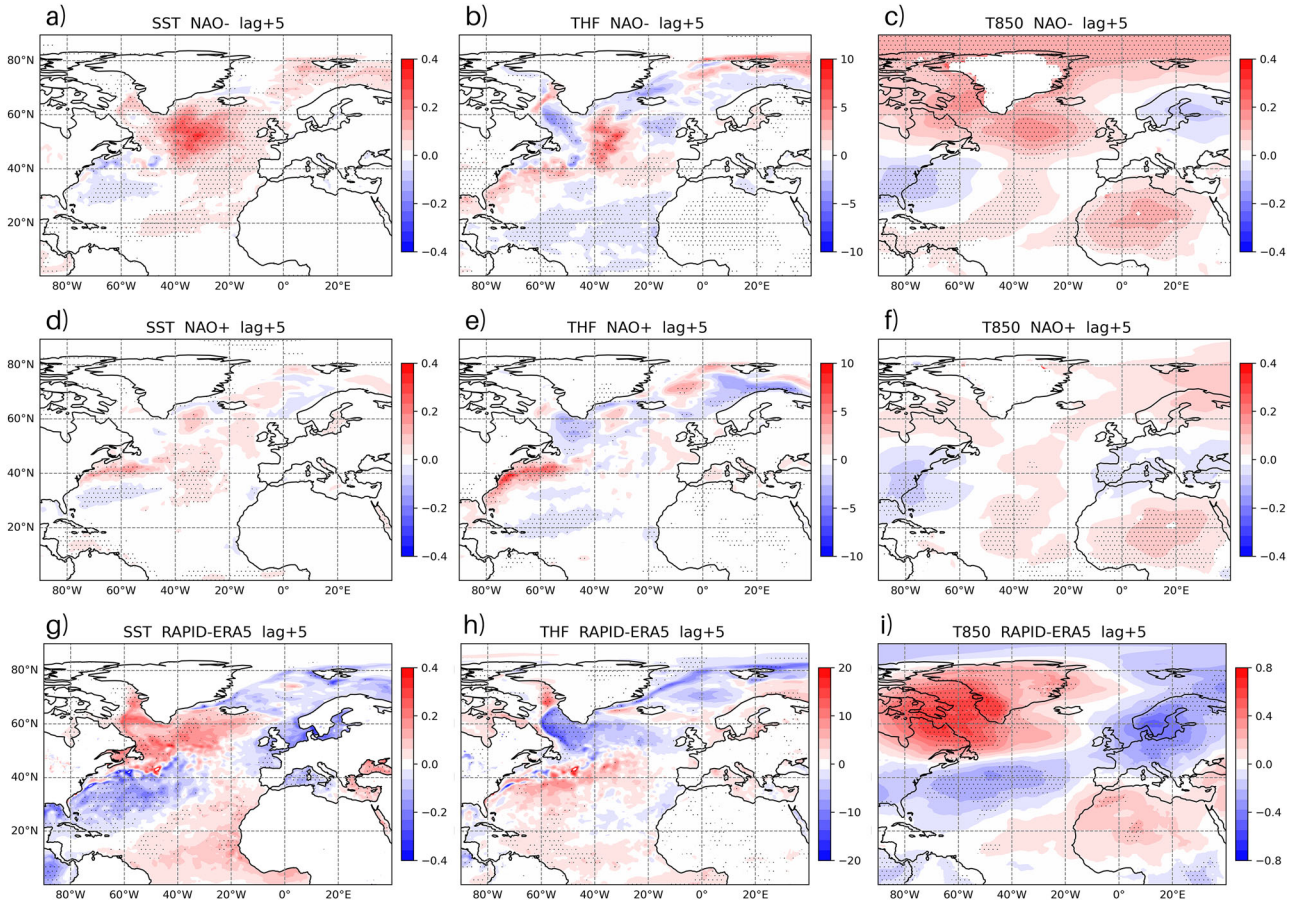

Fig. 3 | Regression AMOC strength on SST, THF and T850. Same as Fig. 2, but now for the regression of AMOC strength at lag +5 on SST (°C Sv^{-1}) (**a**, **d**, **g**) THF (Wm^{-2} Sv^{-1}) (positive is upward) (**b**, **e**, **h**), and temperature at 850 hPa (T850) (°C Sv^{-1}) (**c**, **f**, **i**).

period (1941–2023) supports the ocean warming of the eastern SPG (Fig. S3), corroborating the assessment that ocean forcing is instrumental, although not fully responsible, for the SST/SIC pattern that causes the switch to NAO-sign 5 years after an AMOC peak. For NAO+ THF indicates that the Gulf Stream signal is also forced by ocean advection, warming the atmosphere there (Fig. 3d, e). The precise role of ocean advection is discussed further below.

Further analyses revealed that at lag +1 in NAO− (and NAO+) there is a strong cooling of the Labrador Sea and SPG by the overlying cold air (SST and THF anticorrelated; Fig. S4a, j), whereas in RAPID-ERA5 there is only a weak cooling of the northern Labrador Sea (Fig. S4l) and even ocean warming of the atmosphere in the southern Labrador Sea (SST and THF positively correlated; Fig. S4c, l). At lag +5 in NAO− this has been switched to a weak warming in the Labrador Sea by the atmosphere jointly with warming of the air above of the eastern SPG by the ocean, whereas in RAPID-ERA5 the weak cooling has been switched to a strong warming of the Labrador Sea by the overlying warm air that extends over the SPG as well as shown in Fig. 3.

The forcing of a negative NAO for NAO− at lag +5 by the warm SSTs in the SPG is further supported by the temperature distribution at 850 hPa (Fig. 3c), revealing that the warm SST signal in the SPG is transferred into the lower troposphere by the upward positive THF (Fig. 3b) induced by the warm SSTs. Over the Northern Seas, the anomalous THF is dominated by temperature anomalies, with a minor role for the wind component and specific humidity[30]. Because the atmospheric background state over the baroclinic region consists of a negative meridional temperature gradient (Fig. S5), the warm anomaly over the SPG, together with the cold lower troposphere signal over the Gulf Stream region that is associated with cold SSTs in that region (Fig. 3a, c) south of it, results in a weakening of the meridional temperature gradient in the baroclinic genesis region and thereby a reduction of baroclinic instability as diagnosed by the Eady Growth Rate (EGR) ("Data and methods" section)[31,32] (Fig. S6a, c). As a result of the reduced baroclinic genesis, the storm track as measured by the 2–6 day bandpass-filtered standard deviation of mean sea-level pressure is reduced especially over the eastern flank of the North Atlantic storm track for NAO− (Fig. S6g) which is the region of largest interannual 5-year running mean storm track variability (Fig. S6d). This induces a negative NAO response. RAPID-ERA5 reveals a similar meridional temperature gradient response over the baroclinic genesis region (Fig. 3i), that is also corroborated by the ERA5 data (Fig. S3), inducing a similar reduction in EGR and storm track activity (Fig. S6c, i). NAO+ misses this reduction in the temperature gradient over the jet stream completely (Fig. 3f). The crucial role of the temperature gradient between the SPG and the Gulf Stream for the forcing of a negative NAO at lag +5 is further revealed in Fig. S7 showing a linear relationship between this gradient and the NAO for the High-ResMIP models.

Mechanism of AMOC forced by the NAO at negative lag and the role of bias

The difference in model behaviour between NAO+ and NAO− can be understood in terms of model bias (Fig. 4). Because the simulations are forced with 1950s concentrations of GHG and aerosols[33], the bias is computed with respect to the 1940–1960 period of ERA5. Both ensembles are characterised by a cold bias over the North Atlantic (Fig. 4a, d) and too much SIC (Fig. 4b, e). However, in the NAO+ ensemble, the cold bias is much more severe, especially in the central SPG, and the Labrador Sea and Nordic Seas, and there is a larger sea-ice extent in the Labrador Sea and between Svalbard and Scandinavia. The cold bias and larger sea-ice extent reduce the

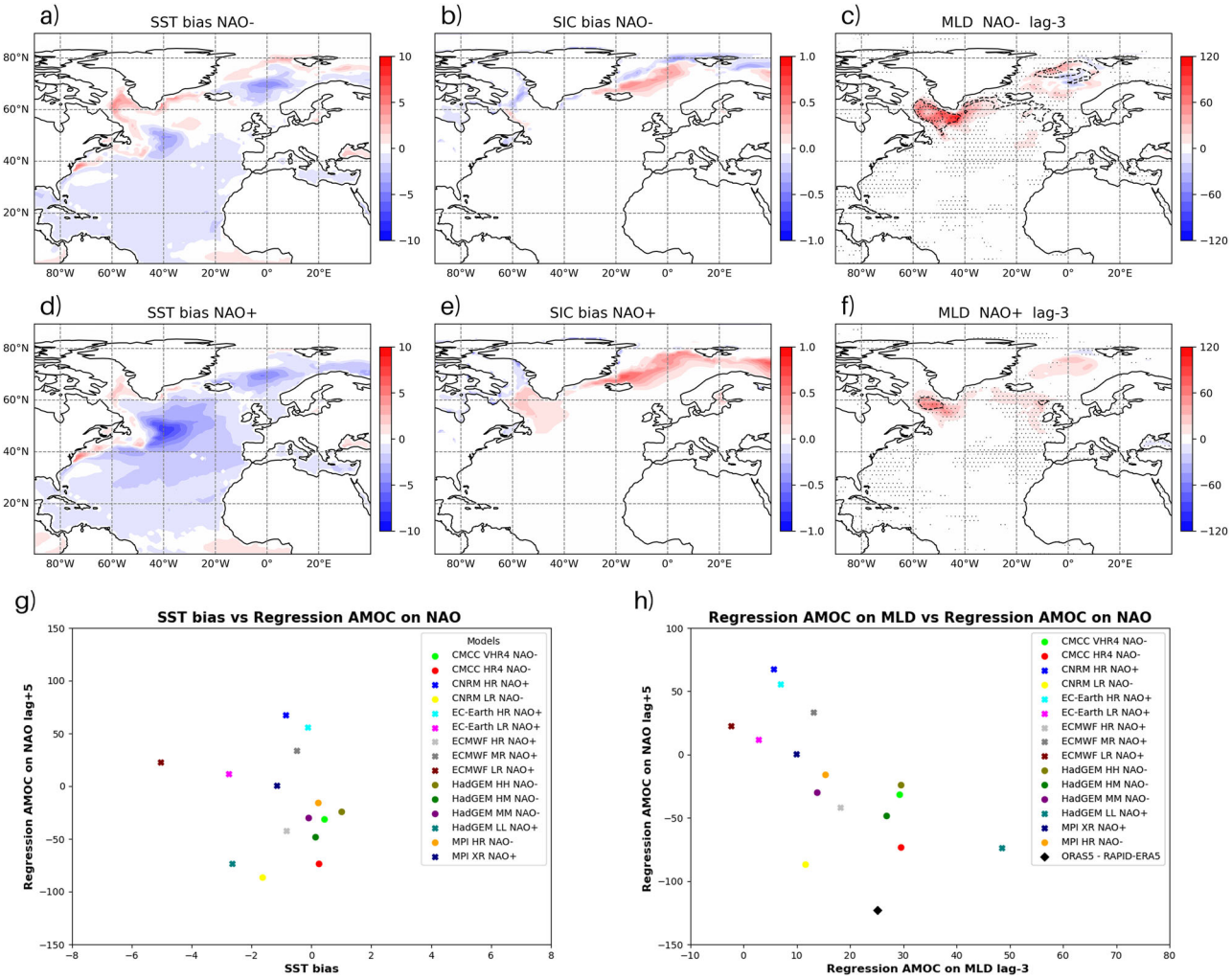

Fig. 4 | Model bias, deep-water formation and NAO response. Model mean bias of NAO− (**a**, **b**) and NAO+ (**d**, **e**) models with respect to 1940–1960 of ERA5. **a**, **d** SST (°C) and **b**, **e** SIC (%). Regression of AMOC strength at 26.5° N ("Data and methods" section) on mixed-layer depth (m Sv^{-1}) at lag −3 of model mean of NAO− (**c**) and NAO+ (**f**) models. Dashed and dotted lines are the climatological MLD depth contours of 500 and 1000 m, respectively (**c** and **f**). Scatter plots of the AMOC at 26.5° N regressed on the NAO (not normalised) (Pa Sv^{-1}) at lag +5 (vertical axis) on **g** the SST bias (°C) in the region of DWF (55 W–40 W, 50 N–60 N) (horizontal axis) and **h** the AMOC at 26.5° N regressed on the mixed-layer depth (MLD) (m Sv^{-1}) (as a proxy for deep-water formation (DWF)) at lag −3 (horizontal axis). The crosses belong to the NAO+ ensemble and the circles to NAO−. The black diamond in (**h**) is RAPID-ERA5/ORAS5.

mean MLD and subsequently also the NAO-forced increase in MLD[22,23] in those regions at negative lags preceding a peak in the AMOC (Fig. 4c, f). We note here that for SIC < 1, periods of ice-free ocean and DWF are still possible due to natural variability because the SIC values are seasonal means with 5-year running means. The reduction of the MLD response to the increasingly positive NAO that leads the AMOC peak (Fig. 1) diminishes the AMOC response to NAO forcing in NAO+. The bias in this group of models also inhibits the strengthening of the positive NAO-signal at the surface associated with forcing an AMOC peak, even when this signal fully appears in the mid-troposphere. This is caused by the cold-high warm-low response at the surface, where an anomalous cold-high pressure system develops over a cold surface that counteracts a positive NAO (Fig. S8). The scatter plot of SST-SPG bias versus lagged regression with NAO at lag +5 (Fig. 4g) reveals a clear relationship between SST bias and the ability of the ocean to force a negative NAO response. The only NAO− model that has a strong negative SST bias is CNRM-LR. Summarising, in most of the models a strong cold bias and larger sea-ice in the northern North Atlantic reduces the ability of a positive NAO to induce strong increases in MLD that is associated with DWF and thereby to force the AMOC that then ultimately induces a negative NAO response.

Dynamics of ocean response

The bias and different AMOC–NAO relations are also reflected in the extent to which AMOC-driven SST anomalies propagate northward. Figures 1–3 show in NAO− and RAPID-ERA5 how AMOC and NAO combine to form an interacted variation that remains coherent over ca. 8 years starting at lag −3. In the NAO− ensemble and RAPID-ERA5 we see at lag −3 already a warm subtropical gyre (STG), but still a cold SPG (Fig. 5a, g). This results in a cooling of the air over the SPG (Fig. S9a), together with a warming of air over the STG. This results in an enhancement of the tropospheric meridional temperature gradient over this nursery of Atlantic storms (Fig. S5) and a reinforcement of storm tracks and the North Atlantic jet stream. The associated increase in northward Ekman transport (Fig. S10) helps advecting the warm SSTs from the STG over the intergyre boundary into the SPG: at lag 0 the warm SST anomaly starts invading the SPG via the eastern branch of the SPG (Fig. 5b, h). At lag +3 the warm anomaly completely fills the SPG (Fig. 5c, i). On the contrary in the NAO+ ensemble, the Gulf Stream is still cold at lag −3 and there is only a weak positive anomaly in the centre of the STG and along the eastern boundary of the Atlantic. At lag 0 both Gulf Stream and STG are warm but no sign of the warm SSTs invading the SPG. At lag +3 the warm SST anomaly remains confined to the northern

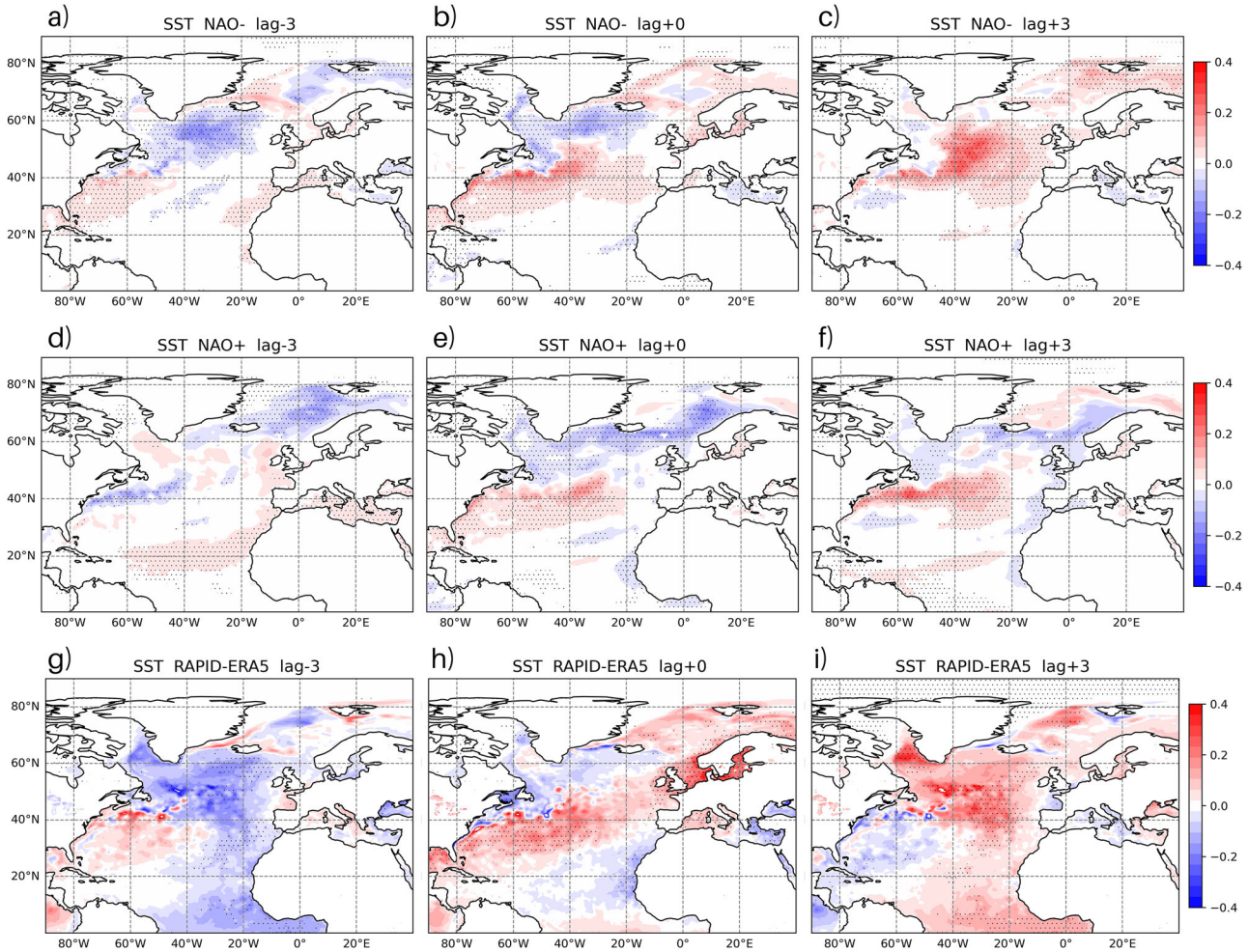

Fig. 5 | Regression of AMOC strength on SST. Regression of AMOC strength at 26.5° N on SST (°C Sv^{-1}). **a**–**c** model mean of NAO− models; **d**–**f**, model mean of NAO+ models; **g**–**i**, RAPID-ERA5. **a**, **d**, **g** lag −3. **b**, **e**, **h** lag 0. **c**, **f**, **i** lag +3. The regressions are computed for the winter season (DJF) with a running mean of 5 years.

boundary of the STG and the SPG remains cold (Fig. 5f). This lack of northward propagation of SSTs in NAO+ is further corroborated by the much weaker Ekman response that increases northward advection in NAO − and RAPID-ORAS5 and the more zonal Gulf Stream extension/North Atlantic Drift in NAO+ compared with NAO− and ORAS5 (Fig. S11). Thus, the different behaviour in the two ensembles is reflected by a lack of northward propagation of SST anomalies from the STG into the SPG during an intensification of the AMOC for the NAO+ models which is associated with a lack of forcing at subpolar latitudes from ocean to atmosphere, necessary for reversing the positive NAO to a negative NAO.

Discussion

The whole chain of processes leading to an interactive variation in NAO and AMOC that roughly ranges from 3 years before to 5 years after a positive AMOC peak is summarised in Fig. 6. This interactive chain is present in NAO− and observations but weak in the NAO+ group in the phase where the NAO forces the AMOC (between lag −3 and lag 0) and completely absent in the phase between lag 0 and lag +5 where mutual feedbacks drive warming in the SPG and Nordic Seas that induce a sign change of the NAO 5 years after an AMOC peak in NAO− and the observations. The main reason for this different behaviour in the NAO− and NAO+ models is the larger cold bias in the SPG and larger SIC-bias in SPG, Labrador Sea and Nordic Seas in NAO+, which hinders a strong MLD and related DWF response to a positive NAO and also counteracts the strengthening of a positive NAO in the build-up to a stronger AMOC. This, on its turn, diminishes the AMOC response to positive NAO forcing. For NAO+ models the weaker AMOC response to the NAO is insufficient to initiate the poleward advection of subtropical SSTs (dark thin blue arrows and red cross in Fig. 6), and the subsequent chain of SPG warming and reduction in atmospheric meridional temperature gradient leading to a reduction of baroclinic instability and weakening of the storm track over the eastern flank of the North Atlantic that results in a negative NAO response about 8 years after the DWF response to a positive NAO and 5 years after an AMOC peak (Fig. 6). The lag −3 of DWF with respect to the AMOC is explained by the time it takes for the induced density changes at high-latitudes to propagate via advection and Kelvin wave equatorward to affect the AMOC at 26.5° N. The lag +5 of SPG SST and NAO response with respect to the AMOC is due to the necessary time for poleward advection of warm subtropical water by the enhanced AMOC and Ekman transport into the SPG. The crucial role of the bias and associated DWF response in forcing a negative NAO about 8 years later is demonstrated by a clear linear relationship between the amount of deepening of the MLD at lag −3 and the NAO response at lag +5 (Fig. 4h). This result is supported by RAPID-ERA5/ORAS5 data (Fig. 4h). A cautionary note to be made is that RAPID-ERA5/ORAS5 only covers a period of 18 years, inhibiting a rigorous statistical analysis. However, using 40 years of ERA5 data still reveals that the SPG is warmed by the ocean (Fig. S3), similar as the lagged regressions on AMOC from the RAPID-ERA5 period suggest.

This storyline focuses at lag −3 on the NAO impact on DWF via temperature-forcing in accordance with previous studies[2]. Also, haline processes play a role in the DWF response. At lag −3 sea surface salinity (SSS) patterns between NAO+, NAO− and RAPID-ORAS5 are quite

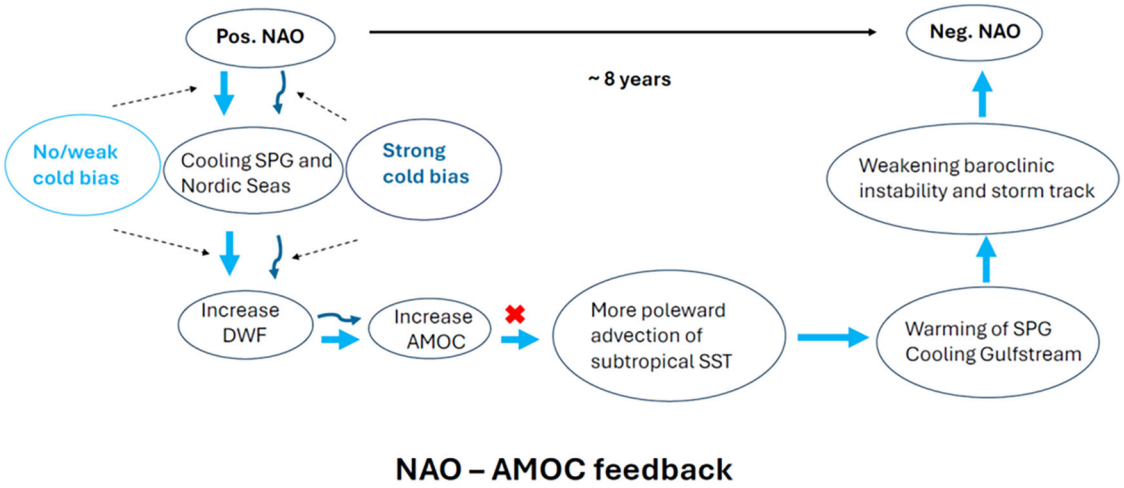

Fig. 6 | NAO–AMOC feedback mechanism. Schematic picture of the NAO–AMOC feedback mechanism. The thick/thin blue arrows indicate the chain of processes for the NAO−/NAO+ models. The red cross indicates the end of the chain of processes for the NAO+ models.

diverse (Fig. S12). Comparing SSS with patterns at larger negative lags excluded northward propagation of these anomalies from a southern origin. The link (regression) between NAO and sea-ice and precipitation also does not support an origin of these anomalies based on changes in brine rejection or surface fluxes. Our (tentative) conclusion is that in the Labrador Sea and Nordic Seas, the signal associated with enhanced DWF is a response to enhanced deep convection and increased upward transfer of positive salinity anomalies during periods of enhanced convection and thus associated with a positive convective feedback.

With roughly 50% of the models used in HighResMIP being able to simulate this coupled AMOC–NAO interaction with ocean and atmosphere mutually forcing each other, and the other 50% not, it is tentative to assume that model resolution is crucial here. This is partly the case, as the real driver of the model differences in simulating this ocean–atmosphere interaction is determined by model bias. When stratifying the different model behaviour versus resolution a mixed picture emerges (Table S1). The NAO− ensemble indeed is mainly, but not exclusively populated by the highest resolution models. We hypothesise that resolution helps to reduce the cold bias. It has been shown that eddy-permitting ocean models reduce the North Atlantic cold bias, due to enhanced poleward heat transport by better representation of ocean dynamics[34]. However, sometimes a low-resolution model, such as CNRM-LR, may have undergone extensive tuning that reduces the impact of cold bias on the processes discussed here.

The AMOC–NAO interaction we find in models and data might be part of a decadal oscillation as has been found in one model[24] and would be a topic for further research, although the process chain illustrated in Fig. 6 appears much weaker when the signs are reversed. Even then, our results imply an important perspective for decadal prediction systems. Unfortunately, at present most decadal prediction systems use model versions of intermediate resolution or less and are part of the NAO+ ensemble in which the physical mechanisms that would support such predictability are absent or degraded. On the other hand, our results imply that targeted tuning to reduce the cold bias in the North Atlantic SPG and Nordic Seas is the most prospecting route for increasing predictive skill.

Data and methods

Models and data. Six Global Climate Models (GCMs) models from the EU-funded Horizon 2020 PRIMAVERA project are investigated. The analysed GCMs are HadGEM3-GC31[35], ECMWF-IFS[36], EC-Earth3P[37], CNRM-CM6[38], MPI-ESM1-2[39] and CMCC-CM2[40]. Each GCM has different configurations. They are, together with their characteristics, summarised in Table 1. For each configuration, one member is analysed. The differences between the configurations of each model are limited to the horizontal resolution of the atmosphere, ocean or both components.

Table 1 | Models that are analysed in this study

Model	Atmos. resol. (km)		Ocean resol. (degrees)
	Effective	Nominal	
CMCC VHR4	182	25	0.25°
CMCC HR4	571	100	1°
CNRM HR	313	50	0.25°
CNRM LR	≥625	250	1°
EC-Earth HR	238	50	0.25°
EC-Earth LR	351	100	1°
ECMWF HR	185	25	0.25°
ECMWF MR	≥185	50	0.25°
ECMWF LR	253	50	1°
HadGEM HH	≤185	50	0.083°
HadGEM HM	185	50	0.25°
HadGEM MM	364	100	0.25°
HadGEM LL	≥625	250	1°
MPI XR	256	50	0.25°
MPI HR	364	100	1°

Third and fourth columns are the nominal resolutions for the atmosphere and ocean, respectively. The second column is the effective resolution for the atmosphere[41].

For these models, 100-year coupled simulations at "1950" conditions following the HighResMIP protocol[33] have been analysed. The constant forcing consists of greenhouse gases and aerosols loading for 1950s climatology (fixed values). Initialisation was provided by a 50-year spin-up integration, with fixed forcing representative of the 1950s starting from the observed ocean and atmosphere state in 1950.

The model nominal resolution based on grid point distance is less than the effective resolution which estimates the scales that are not affected by the horizontal resolution. The latter is usually determined by the deviation of the simulated kinetic energy spectrum from the observed k^{-3} spectrum, where k is the total wavelength. For the GCMs used in this study, the effective resolution[41] is also listed in Table 1. The effective resolution is about 3–5 times the nominal resolution. For the ocean components a similar analysis is not available, but we assume that a similar ratio applies.

In addition, we analysed the ERA5 reanalysis[42] for the period 1941–2023, the ORAS5 ocean reanalysis[43] for the period 1958–2023, and the RAPID array data[44] which is available for the period 2004–2022. Over the Nordic Seas, the turbulent surface heat fluxes of ERA5 compare well to in-

situ observations and satellite estimates[45]. Only over the marginal ice zones, the correspondence is noticeably less accurate due to the overly smooth sea-ice distribution in the surface boundary conditions used in ERA5[45].

Analyses. The analyses have been done for winter (December–February, DJF) seasonal means. During this season NAO is well-defined and atmosphere-ocean coupling strongest. To remove spurious trends second-order nonlinear detrending has been applied before the analyses. All analyses have been done with a 5-year running mean applied on the DJF data.

Both for the models and the RAPID array data the AMOC strength at 26.5° N is obtained by integrating the meridional transport at 26.5° N across the Atlantic basin (zonally) and then doing a cumulative integral in depth. The maximum value in depth is then taken as the strength in Sverdrups ($1\ \mathrm{Sv} = 10^6\ \mathrm{m}^3\ \mathrm{s}^{-1}$). Before the analyses, the atmospheric data have been regridded to a regular lat-lon grid of 1×1 degree. The NAO is computed by the normalised difference between the MSLP averaged over a southern box (20 N–50 N, −60 E–20 E) and a northern box (55 N–85 N, −60 E–20 E) over the Atlantic and Western Europe. The normalisation is done by scaling with the area mean standard deviation over the respective boxes. The anomalies are computed with respect to DJF.

The change in MLD, which is associated with the change in subduction, is used here as a proxy for the change in DWF.

To analyse baroclinic genesis the EGR[31] σ is used:

$$\sigma = 0.31 \quad (f/N) \quad \left(\frac{\partial U}{\partial Z}\right)$$

where f is the Coriolis parameter, N the static stability, Z the geopotential height and U the zonal velocity. The EGR is computed between the 850- and 700-hPa levels using monthly mean data of air temperature, geopotential height and horizontal wind[32].

Statistical significance is computed using a student's two-tailed t-test and a p value of 0.05. The effective sample size is $N^* = N(1 - \mathrm{r1} \cdot \mathrm{r2})/(1 + \mathrm{r1} \cdot \mathrm{r2})$ where N denotes the length of time series and r1 and r2 denote lag-one autocorrelation coefficients of either variable[46]. Because the autocorrelation for the 5-year running mane variables is about 0.8 this results in an effective sample size of 22 for the 100-year coupled runs and 4 for the 18-year RAPID-ERA5/ORAS5 data.

Data availability

All data used in this study can be retrieved from publicly available repositories: Data of the climate model simulations from the Earth System Grid Federation (ESGF) nodes: https://esgf.llnl.gov/. ERA5 atmosphere reanalyses data: https://climate.copernicus.eu/climate-reanalysis. ORAS5 ocean reanalyses data: https://cds.climate.copernicus.eu/cdsapp#!/dataset/reanalysis-oras5?tab=form. RAPID data: https://www.rapid.ac.uk/rapidmoc/.

Code availability

The source codes used in this study are available from the corresponding author upon request.

Received: 8 July 2024; Accepted: 11 February 2025;
Published online: 20 February 2025

References

1. Polo, I., Robson, J., Sutton, R. & Balmaseda, M. A. The importance of wind and buoyancy forcing for the boundary density variations and the geostrophic component of the AMOC at 26° N. *J. Phys. Oceanogr.* **44**, 2387–2408 (2014).
2. Delworth, T. L. & Greatbatch, R. J. Multidecadal thermohaline circulation variability driven by atmospheric surface flux forcing. *J. Clim.* **13**, 1481–1495 (2000).
3. Eden, C. & Willebrand, J. Mechanism of interannual to decadal variability of the North Atlantic circulation. *J. Clim.* **14**, 2266–2280 (2001).
4. Eden, C. & Jung, T. North Atlantic interdecadal variability: oceanic response to the North Atlantic Oscillation (1865–1997). *J. Clim.* **14**, 676–691 (2001).
5. Buckley, M. W. & Marshall, J. Observations, inferences, and mechanisms of the Atlantic Meridional Overturning Circulation: a review. *Rev. Geophys.* **54**, 5–63 (2016).
6. Zhao, J. & Johns, W. Wind-forced interannual variability of the Atlantic Meridional Overturning Circulation at 26.5° N. *J. Geophys. Res. Oceans* **119**, 2403–2419 (2014).
7. Frankignoul, C., Gastineau, G. & Kwon, Y.-O. The influence of the AMOC variability on the atmosphere in CCSM3. *J. Clim.* **26**, 9774–9790 (2013).
8. Wills, R. C. J., Armour, K. C., Battisti, D. S. & Hartmann, D. L. Ocean–atmosphere dynamical coupling fundamental to the Atlantic multidecadal oscillation. *J. Clim.* **32**, 251–272 (2019).
9. Frankignoul, C., Gastineau, G. & Kwon, Y.-O. Wintertime atmospheric response to North Atlantic ocean circulation variability in a climate model. *J. Clim.* **28**, 7659–7677 (2015).
10. Gastineau, G., L'Hévéder, B., Codron, F. & Frankignoul, C. Mechanisms determining the winter atmospheric response to the Atlantic overturning circulation. *J. Clim.* **29**, 3767–3785 (2016).
11. Peings, Y. & Magnusdottir, G. Forcing of the wintertime atmospheric circulation by the multidecadal fluctuations of the North Atlantic ocean. *Environ. Res. Lett.* **9**, 034018 (2014).
12. Booth, B. B. B., Dunstone, N. J., Halloran, P. R., Andrews, T. & Bellouin, N. Aerosols implicated as a prime driver of twentieth-century North Atlantic climate variability. *Nature* **484**, 228–232 (2012).
13. Bellomo, K., Murphy, L. N., Cane, M. A., Clement, A. C. & Polvani, L. M. Historical forcings as main drivers of the Atlantic multidecadal variability in the CESM large ensemble. *Clim. Dyn.* **50**, 3687–3698 (2018).
14. Clement, A. et al. The Atlantic Multidecadal Oscillation without a role for ocean circulation. *Science* **350**, 320–324 (2015).
15. Cane, M. A., Clement, A. C., Murphy, L. N. & Bellomo, K. Low-pass filtering, heat flux, and atlantic multidecadal variability. *J. Clim.* **30**, 7529–7553 (2017).
16. Bellucci, A., Mariotti, A. & Gualdi, S. The role of forcings in the twentieth-century North Atlantic multidecadal variability: the 1940–75 North Atlantic cooling case study. *J. Clim.* **30**, 7317–7337 (2017).
17. Zhang, R. et al. A review of the role of the Atlantic meridional overturning circulation in Atlantic multidecadal variability and associated climate impacts. *Rev. Geophys.* **57**, 316–375 (2019).
18. Ting, M., Kushnir, Y. & Li, C. North Atlantic multidecadal SST oscillation: external forcing versus internal variability. *J. Mar. Syst.* **133**, 27–38 (2014).
19. Peings, Y., Simpkins, G. & Magnusdottir, G. Multidecadal fluctuations of the North Atlantic Ocean and feedback on the winter climate in CMIP5 control simulations. *J. Geophys. Res. Atmos.* **121**, 2571–2592 (2016).
20. Kravtsov, S. Pronounced differences between observed and CMIP5-simulated multidecadal climate variability in the twentieth century. *Geophys. Res. Lett.* **44**, 5749–5757 (2017).
21. Kim, W. M., Yeager, S., Chang, P. & Danabasoglu, G. Low-frequency North Atlantic climate variability in the community earth system model large ensemble. *J. Clim.* **31**, 787–813 (2018).
22. Kim, H.-J. et al. North Atlantic oscillation impact on the Atlantic meridional overturning circulation shaped by the mean state. *Npj Clim. Atmos. Sci.* **6**, 1–13 (2023).
23. Reintges, A., Robson, J. I., Sutton, R. & Yeager, S. G. Subpolar North Atlantic mean state affects the response of the Atlantic Meridional Overturning Circulation to the North Atlantic oscillation in CMIP6 models. *J. Clim.* **37**, 5543–5559 (2024).

24. Wen, N., Frankignoul, C. & Gastineau, G. Active AMOC–NAO coupling in the IPSL-CM5A-MR climate model. *Clim. Dyn.* **47**, 2105–2119 (2016).
25. Wang, C., Zhang, L., Lee, S.-K., Wu, L. & Mechoso, C. R. A global perspective on CMIP5 climate model biases. *Nat. Clim. Change* **4**, 201–205 (2014).
26. Gastineau, G. & Frankignoul, C. Influence of the North Atlantic SST variability on the atmospheric circulation during the twentieth century. *J. Clim.* **28**, 1396–1416 (2015).
27. Davini, P., Hardenberg, Jvon & Corti, S. Tropical origin for the impacts of the Atlantic multidecadal variability on the Euro-Atlantic climate. *Environ. Res. Lett.* **10**, 094010 (2015).
28. Yu, L. & Weller, R. A. Objectively analyzed air–sea heat fluxes for the global ice-free oceans (1981–2005). *Bull. Am. Meteorol. Soc.* **88**, 527–540 (2007).
29. Comment on "The Atlantic Multidecadal Oscillation without a role for ocean circulation". *Science* **352**, 1527 (2016).
30. Zhang, Z.-L. et al. On the turbulent heat fluxes: a comparison among satellite-based estimates, atmospheric reanalyses, and *in-situ* observations during the winter climate over Arctic sea ice. *Adv. Clim. Change Res.* **14**, 347–362 (2023).
31. Hoskins, B. J. & Valdes, P. J. On the existence of storm-tracks. *J. Atmos. Sci.* **47**, 1854–1864 (1990).
32. Athanasiadis, P. J. et al. Mitigating climate biases in the midlatitude North Atlantic by increasing model resolution: SST gradients and their relation to blocking and the jet. *J. Clim.* **35**, 6985–7006 (2022).
33. Haarsma, R. J. et al. High resolution model intercomparison project (HighResMIP v1.0) for CMIP6. *Geosci. Model Dev.* **9**, 4185–4208 (2016).
34. Moreno-Chamarro, E. et al. Impact of increased resolution on long-standing biases in HighResMIP-PRIMAVERA climate models. *Geosci. Model Dev.* **15**, 269–289 (2022).
35. Roberts, M. J. et al. Description of the resolution hierarchy of the global coupled HadGEM3-GC3.1 model as used in CMIP6 HighResMIP experiments. *Geosci. Model Dev.* **12**, 4999–5028 (2019).
36. Roberts, C. D. et al. Climate model configurations of the ECMWF Integrated Forecasting System (ECMWF-IFS cycle 43r1) for HighResMIP. *Geosci. Model Dev.* **11**, 3681–3712 (2018).
37. Haarsma, R. et al. HighResMIP versions of EC-Earth: EC-Earth3P and EC-Earth3P-HR – description, model computational performance and basic validation. *Geosci. Model Dev.* **13**, 3507–3527 (2020).
38. Voldoire, A. et al. Evaluation of CMIP6 DECK experiments with CNRM-CM6-1. *J. Adv. Model. Earth Syst.* **11**, 2177–2213 (2019).
39. Gutjahr, O. et al. Max Planck Institute Earth System Model (MPI-ESM1.2) for the High-Resolution Model Intercomparison Project (HighResMIP). *Geosci. Model Dev.* **12**, 3241–3281 (2019).
40. Cherchi, A. et al. Global mean climate and main patterns of variability in the CMCC-CM2 coupled model. *J. Adv. Model. Earth Syst.* **11**, 185–209 (2019).
41. Klaver, R., Haarsma, R., Vidale, P. L. & Hazeleger, W. Effective resolution in high resolution global atmospheric models for climate studies. *Atmos. Sci. Lett.* **21**, e952 (2020).
42. Hersbach, H. et al. The ERA5 global reanalysis. *Q. J. R. Meteorol. Soc.* **146**, 1999–2049 (2020).
43. Zuo, H., Balmaseda, M. A., Tietsche, S., Mogensen, K. & Mayer, M. The ECMWF operational ensemble reanalysis–analysis system for ocean and sea ice: a description of the system and assessment. *Ocean Sci.* **15**, 779–808 (2019).
44. Moat, B. I. et al. Atlantic meridional overturning circulation observed by the RAPID-MOCHA-WBTS (RAPID-Meridional Overturning Circulation and Heatflux Array-Western Boundary Time Series) array at 26N from 2004 to 2020 (v2020.2). https://nora.nerc.ac.uk/id/eprint/535061/ (2023).
45. Renfrew, I. A. et al. An evaluation of surface meteorology and fluxes over the Iceland and Greenland Seas in ERA5 reanalysis: the impact of sea ice distribution. *Q. J. R. Meteorol. Soc.* **147**, 691–712 (2021).
46. Bretherton, C. S., Widmann, M., Dymnikov, V. P., Wallace, J. M. & Bladé, I. The effective number of spatial degrees of freedom of a time-varying field. *J. Clim.* **12**, 1990–2009 (1999).

Acknowledgements

R.H. was supported by the EERIE Project (Grant Agreement ID 101081383) of the EU Horizon Europe Framework Programme. S.D. was supported by WISHBONE and ArctiConnect. We thank Hylke de Vries, Jordi Beunk and Tom Assendelft for their help in post-processing and analysing the data. Data from the RAPID AMOC monitoring project are funded by the Natural Environment Research Council and are freely available from www.rapid.ac.uk/rapidmoc.

Author contributions

R.H. performed the analyses. R.H. and S.D. contributed both to the development of the scientific content and writing of the article.

Competing interests

The authors declare no competing interests.

Additional information

Supplementary information The online version contains supplementary material available at https://doi.org/10.1038/s43247-025-02123-5.

Correspondence and requests for materials should be addressed to Rein Haarsma.

Peer review information *Communications Earth & Environment* thanks the anonymous reviewers for their contribution to the peer review of this work. Primary handling editors: Jennifer Veitch and Alireza Bahadori. A peer review file is available.